Air-Stable, Efficient Mixed-Cation Perovskite Solar Cells with Cu Electrode by Scalable Fabrication of Active Layer

*Yehao Deng, Qingfeng Dong, Cheng Bi, Yongbo Yuan, and Jinsong Huang**

Organic–inorganic halide perovskite solar cells have reached over 21.0% power conversion efficiency (PCE) in only a few years of development due to their extraordinary and unique optoelectronic properties such as long carrier diffusion length.[1–3] Next big challenges to be addressed for perovskite solar cells are the scalable fabrication and long term stability before they can be considered for real products. One advantage of perovskite materials over Si and Gallium Arsenide (GaAs) for large area solar cell application is their solution process capability, which allows us to leverage the existing scalable solution deposition methods established in many other fields, such as slot-die coating and roll-to-roll fabrication, for large area perovskite solar cell fabrication. Though the state-of-the-art perovskite solar cells have multiple layers including charge transport layers,[4–6] the capability to fabricate a high quality perovskite layer by these scalable methods is crucial, because the fabrication of charge transport layers, including both organic and inorganic nanoparticle layers, have been well-established in the research of organic solar cells.[7,8] In the past couple of years, some efforts have been devoted to searching a good scalable deposition method for the perovskite layers, including spray-coating,[9] electrochemical deposition,[10] doctor-blade coating,[11,12] slot-die coating,[13] etc. However the device efficiencies from all these scalable deposition methods still lag far behind the state-of-the-art spin-coated devices by 30%–50%. The reasons include incomplete perovskite film coverage, presence of pin-holes, and high roughness at grain scale caused by less controlled nucleation and/or crystal growth and the limited attempts of perovskite composition engineering in scalable fabrication methods.[14–16] In addition, scalable fabrication method should come with good long term stability to make perovskite solar cells a real solution to renewable energy conversion. Among many degradation mechanisms,[17,18] the interface deterioration by chemical reaction between the perovskite layer and the metal electrode (e.g., Al, Ag) in the ambient environment have been reported to dominate the initial degradation of perovskite solar cells,[19] which occurs far ahead of the degradation of perovskite grains by moisture or heat. Several recent studies showed that spatially separating the perovskite layer and metal cathode could significantly slow down the interface breakdown by increasing the thickness of fullerene electron transporting layer (ETL) or replacing this layer by compact ZnO ETL.[20,21] However, fundamental solution to this problem still relies on finding another electrode material which is much less reactive with perovskite. Gold (Au) is chemically less active than Al and Ag, but the chemical reaction between Au and perovskite at the interface level is still observed,[19] not to mention the high price of Au.

Here, we report the fabrication of compact, smooth at grain scale, and pure phase of mixed cation (formamidinium (FA) and methylammonium (MA)) perovskite films by doctor-blade coating method. The mixed cation perovskite is chosen because of its lower bandgap for potentially higher device efficiency, as demonstrated by previous studies using the nonscalable fabrication process.[2] The compositionally tuned perovskite layer extends the absorption onset to 850 nm, resulting in an increased PCE of over 18.0%, which is comparable to that of the spin-coated devices. In addition, we improved the devices stability substantially by replacing Al with Cu as cathode. The unsealed devices stored in ambient condition of ≈25 °C with 20%–60% relative humidity could maintain the performance without any PCE loss for up to 20–30 d.

Figure 1a illustrates the doctor-blade coating of mixed-cation perovskite $FA_xMA_{1-x}PbI_3$ layer, modified from our previous report.[12] Briefly, PbI_2, methylammonium iodide (MAI) and formamidinium iodide (FAI) were dissolved in *N,N*-dimethylformamide (DMF) at room temperature at a molar ratio of $FAI:MAI:PbI_2 = x:(1\text{-}x):1$. Then the solution was dropped on to preheated (100–145 °C) substrates on a hot plate, and swiped from the front to the end. The perovskite films dried in seconds, and then were removed from the hot plate quickly.

In this study, we first demonstrate that the doctor-blade coating method provides a better control for the $FAPbI_3$ film formation process due to its facile temperature controlling capability. $FAPbI_3$ has two phases, one is black, perovskite α-phase at 2θ of 16° in X-ray diffraction (XRD) pattern by Co-Kα radiation ($\lambda = 1.788$ Å), and the other one is yellow, non-perovskite δ-phase at 2θ of 14.1°. It is well known that $FAPbI_3$ is thermodynamically stable in δ-phase at room temperature, and stable in α-phase at higher temperature.[15,22] The spun $FAPbI_3$ films are often δ-phase (Figure 1b),[15] which requires a high temperature annealing (150 °C, 10–30 min) process to convert them into α-phase (Figure 1c).[15,23] The doctor-bladed $FAPbI_3$ films have the desired α-phase perovskite which can be directly obtained without an additional thermal annealing process, because the precursor solution and the substrates can be heated in situ to the temperature that favors α-phase formation (Figure 1c). Figure 1d shows the X-ray diffraction patterns of pure $FAPbI_3$ ($x = 1$) films prepared at different doctor-blading

Y. Deng, Dr. Q. Dong, C. Bi, Dr. Y. Yuan, Prof. J. Huang
Department of Mechanical and Materials Engineering
University of Nebraska-Lincoln
Lincoln, NE 68588, USA
E-mail: jhuang2@unl.edu

Y. Deng, Dr. Q. Dong, C. Bi, Dr. Y. Yuan, Prof. J. Huang
Nebraska Center for Materials and Nanoscience
University of Nebraska-Lincoln
Lincoln, NE 68588, USA

DOI: 10.1002/aenm.201600372

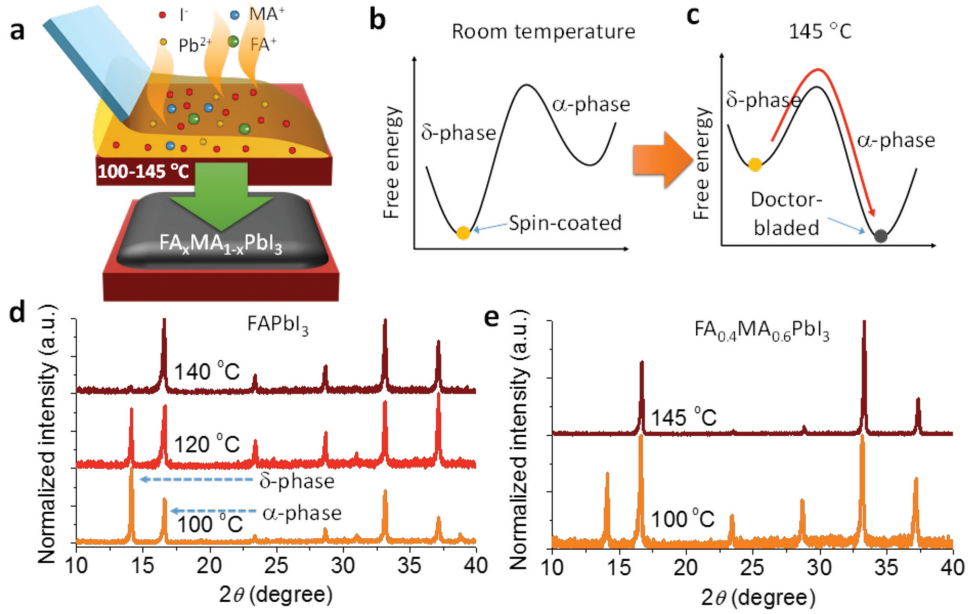

Figure 1. Mixed cation perovskite film formation mechanism. a) Illustration of doctor-blade coating of mixed cation perovskite film from precursor solution heated by a hot plate. b,c) Schematic diagrams of free energy versus α-phase and δ-phase of mixed cation perovskite at room temperature and 145 °C, respectively. d,e) X-ray diffraction patterns for $FAPbI_3$ and $FA_{0.4}MA_{0.6}PbI_3$, respectively, prepared at different doctor-blade coating temperatures.

temperature. When the substrate temperature was increased from 100 to 140 °C, the peak intensity ratio of α-phase to δ-phase on the as-prepared film increased monotonously. When the substrate temperature reached 140 °C, the formed film was mainly composed of α-phase. It should be noted that though a high temperature is still applied during doctor-blade coating, the film formation process takes only several seconds, which is energy/time-saving and thus suitable for scalable fabrication.

Pure α-phase of $FAPbI_3$ is not suitable for stable device application, because it undergoes a slow phase transformation to δ-phase at room temperature.[15,24] In addition, it is found that the film coverage of pure $FAPbI_3$ on the substrate (**Figure 2**a) is not complete, unlike pure $MAPbI_3$,[12] possibly due to the presence of δ-phase in pure $FAPbI_3$ that influences the film morphology, or higher nucleus formation energy and thus slower nucleation rate of $FAPbI_3$ as compared to $MAPbI_3$. We addressed the phase stability and film coverage problems simultaneously by alloying $FAPbI_3$ with $MAPbI_3$. Specifically, a FA:MA molar ratio of 2:3 in the precursor solution resulted in the formation of compact perovskite films with 100% coverage (Figure 2c), as compared to the films made at a FA:MA molar ratio of 0.8:0.2, where big gaps between domains presented (Figure 2b). The domain structure is resulted from Rayleigh–Bénard convection of solution by heated substrate during doctor-blade coating, as we have reported elsewhere.[25] A magnified scanning electron microscopy (SEM) image in Figure S1a (Supporting Information) shows that the films are smooth at the grain scale, which is beneficial for the conformal coating of

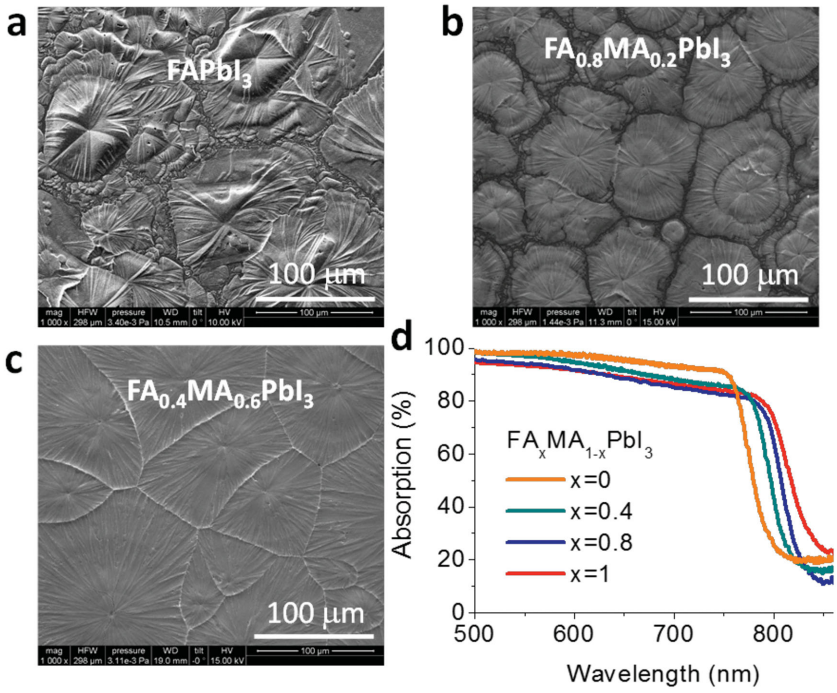

Figure 2. Scanning electron microscopy (SEM) images of mixed cation perovskite films and absorption spectra. a–c) SEM images of $FAPbI_3$, $FA_{0.8}MA_{0.2}PbI_3$, and $FA_{0.4}MA_{0.6}PbI_3$ films prepared by doctor-blade coating at 145 °C. d) Absorption spectra of $FA_xMA_{1-x}PbI_3$ films (x = 0, 0.4, 0.8, 1).

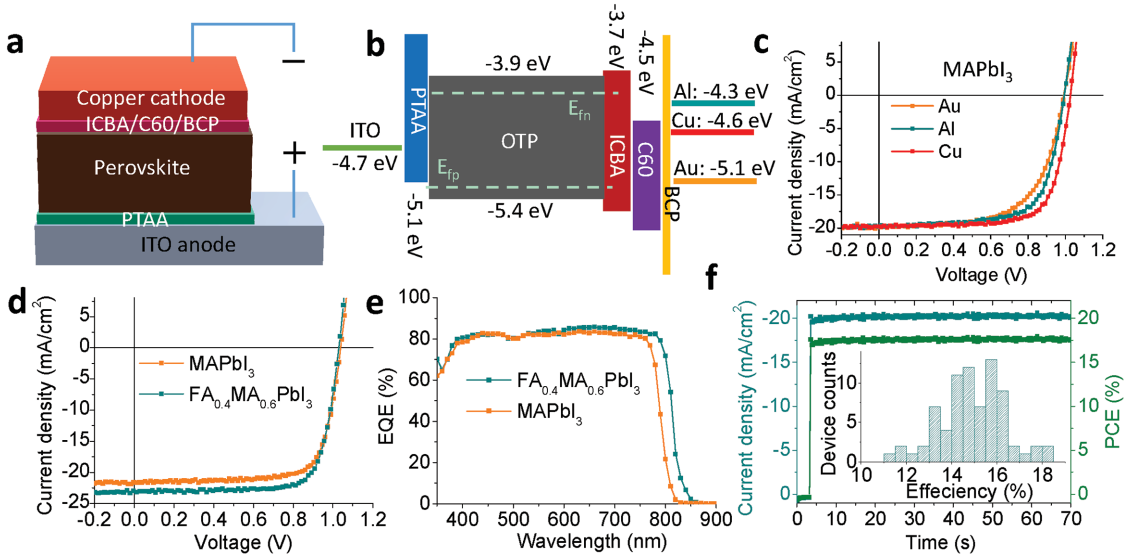

Figure 3. Perovskite solar cell structure and device performances with doctor-bladed active layers. a) Illustration of perovskite solar cell structure. b) Energy level diagram in perovskite solar cell. c) Current density–voltage (J–V) curves of $MAPbI_3$ devices with Au, Al, or Cu cathode. d) J–V curves of champion $MAPbI_3$ and $FA_{0.4}MA_{0.6}PbI_3$ devices with Cu cathode. e) External quantum efficiency (EQE) spectra of $MAPbI_3$ and $FA_{0.4}MA_{0.6}PbI_3$ devices. f) Stabilized photocurrent output at 0.87 bias and calculated power conversion efficiency (PCE) of $FA_{0.4}MA_{0.6}PbI_3$ device. Inset is the PCE statistics of $FA_{0.4}MA_{0.6}PbI_3$ devices.

ETL and the cathode on top of them. In addition, the obtained mixed cation perovskite films by doctor-blade coating at 145 °C could retain its phase purity in ambient environment for more than 20 d (Figure S1b, Supporting Information). It should be noted that though a relatively large percentage of $MAPbI_3$ was alloyed, the absorption edge only blue-shifted by ≈20 nm as compared to that of pure $FAPbI_3$. The band gaps of $FAPbI_3$, $FA_{0.4}MA_{0.6}PbI_3$, and $MAPbI_3$ films calculated by Tauc plot from the absorption spectra are 1.51, 1.55, and 1.60 eV, respectively (Figure S2, Supporting Information).

Perovskite solar cells based on doctor-bladed perovskite layers were fabricated with a device structure of indium tin oxide (ITO)/Poly[bis(4-phenyl)(2,4,6-trimethylphenyl)amine] (PTAA)/perovskite/indene-C60 bisadduct (ICBA)/C_{60}/2,9-dimethyl-4,7-diphenyl-1,10-phenanthroline (BCP)/metal cathode, as is shown in **Figure 3**a.[6] The metal cathodes used here were Al, Cu, and Au. The corresponding energy diagram is shown in Figure 3b. The reason we choose different metal cathodes is to try to improve device stability as shown below, but we first need to make sure alternative metal as the cathode will not sacrifice the device performance. It is interesting that though there is a large work function difference between Al (4.3 eV) and Au (5.1 eV), the performances of the devices based on $MAPbI_3$ photoactive layer were similar under one sun illumination (100 mW cm^{-2}) (Figure 3c). They had almost the same short circuit current (J_{sc}) of 19.8 mA cm^{-2} and open circuit voltage (V_{oc}) of 1.0 V, excepting a lower fill factor (FF) of 63% for the device with Au cathode than 70% of Al device. This is in contrast to organic solar cells, whose V_{oc} shall be reduced by ≈0.4 eV when the cathode is changed from Al to Au as a result of decreased built-in potential according to the metal-dielectric-metal model.[26–28] However, perovskite is different from organic active layer because of its low exciton binding energy and superior carrier transportation capability,[3,29] therefore the anode–cathode work function difference appears not so important for the separation and collection of photogenerated carriers as in organic solar cells. In fact, we have shown previously that a simple device structure of ITO/poly(3,4-ethylenedioxythiophene) poly(styrenesulfonate) (PEDOT:PSS)/perovskite/phenyl-C61-butyric acid methyl ester/Au had an instant V_{oc} of 0.6 V under one sun illumination, though PEDOT:PSS and Au have nearly the same work function.[30] The V_{oc} of such device can further increase to over 1.0 eV when the perovskite layer's quasi-Fermi level splitting is enlarged by "light poling" induced self-doping effect[30] or electric poling induced doping effect.[31,32] Therefore, it is further demonstrated that perovskite solar cells' performance is mainly determined by perovskite layer's intrinsic quasi-Fermi level splitting, as is illustrated in Figure 3b, and the work function of the material for anode/cathode is not essential. Inspired by this, copper was used as the cathode, and the corresponding devices showed similar performance to devices with Al or Au as cathodes (Figure 3c). The slightly improved performance of the device with Cu cathode may be explained by the less reaction of perovskite with Cu than Al, which we will show in the following. We also speculate a less damage to C_{60}/BCP layer during the deposition of Cu than Au, which explains a better device efficiency of the device with Cu cathode than Au cathode.

The champion cells with Cu cathode based on $FA_{0.4}MA_{0.6}PbI_3$ and $MAPbI_3$ perovskite active layers are shown in Figure 3d. The $MAPbI_3$ device had a V_{oc} of 1.04 V, J_{sc} of 21.7 mA cm^{-2} and FF of 75%, yielding a PCE of 16.9%. The $FA_{0.4}MA_{0.6}PbI_3$ device with extended absorption spectrum to 820 nm had a larger J_{sc} of 23.0 mA cm^{-2} without losing V_{oc} (1.03 V) and FF (77%), yielding an enhanced PCE of 18.3%. To the best of our knowledge, this is the highest reported efficiency for devices fabricated by scalable manufacture method. The external quantum efficiency (EQE) spectra in Figure 3e show that the increased J_{sc} of $FA_{0.4}MA_{0.6}PbI_3$ device as compared to $MAPbI_3$ device indeed comes from extended absorption edge from ≈820–850 nm, consistent with

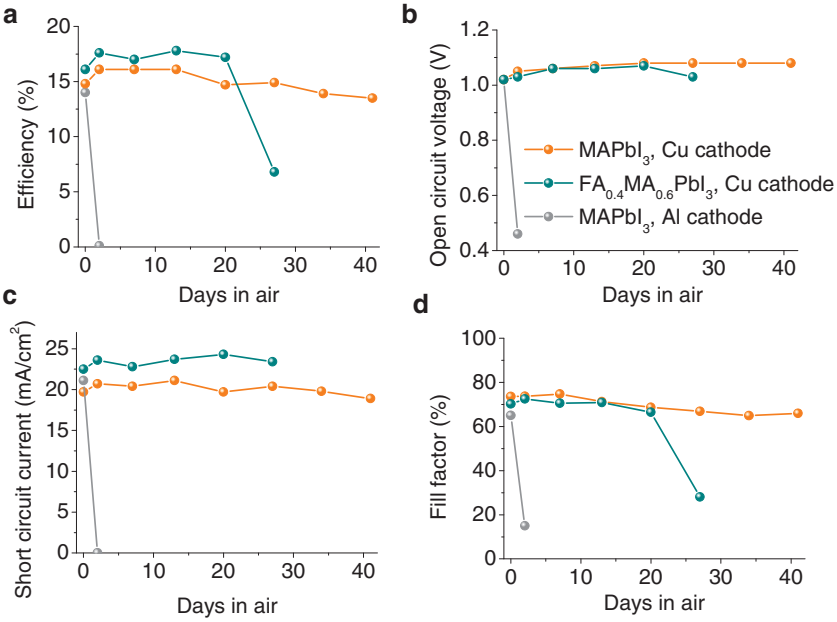

Figure 4. Environmental stability test of unsealed perovskite solar cells. a–d) Variation of PCE, open circuit voltage, short circuit current, and fill factor of perovskite solar cells with different composition and cathode metal with number of days stored in air at ≈25 °C with 20%–60% relative humidity.

the absorption measurement. The current density–voltage (J–V) curves of $MAPbI_3$ and $FA_{0.4}MA_{0.6}PbI_3$ devices scanned in forward and reverse direction are shown in Figure S3 (Supporting Information), showing only a little hysteresis in both devices. Figure 3f shows the stabilized photocurrent of the $FA_{0.4}MA_{0.6}PbI_3$ device at the maximum power output bias (0.87 V) along with calculated PCE. The photocurrent saturated at ≈20.6 mA cm^{-2} right after the light was switched on, giving a stabilized PCE of 18.0% which is close to that derived from J–V curves. The inset in Figure 3f is the PCE statistics of the $FA_{0.4}MA_{0.6}PbI_3$ devices, which shows good reproducibility of this doctor-blade coating method to achieve high PCE perovskite solar cells comparable to those spin-coated devices.[6,33]

The air stability of unsealed devices with Cu cathode was evaluated. They were stored in ambient environment at ≈25 °C with relative humidity of 20%–60%, and their performance change is summarized in **Figure 4** and Figure S4 (Supporting Information). Both $MAPbI_3$ and $FA_{0.4}MA_{0.6}PbI_3$ devices showed good stability with ZERO loss of PCE for up to 30 and 20 d, respectively. Interestingly, a steady increase of V_{oc} was observed during the initial period of storage in both types of devices, leading to PCEs increase at the beginning. This phenomenon may be caused by the reduced charge traps in the bulk of perovskite films due to an aging effect. Possible explanations include water molecule healing effect on perovskite film as is reported elsewhere,[34,35] and detailed study is subject to our further research. In addition, the $MAPbI_3$ devices appeared to be more stable than the $FA_{0.4}MA_{0.6}PbI_3$ devices in air. It might be related to the fact that the MA cation has one less amino group than the FA cation, therefore $MAPbI_3$ is less sensitive to moisture than $FA_{0.4}MA_{0.6}PbI_3$.

In striking contrast, the PCE of the device with Al cathode dropped to near zero after storing it in air for only 2 d (Figure 4 and Figure S5, Supporting Information). It can be ascribed to the fact that perovskite is much more stable with Cu than Al (and Ag). When Al or Ag thin films were deposited directly onto perovskite films, the metallic films became gray and lusterless in several minutes after opening the thermal evaporation chamber and exposing the metal/perovskite stacking layers to air (inset in **Figure 5**a). In the XRD patterns of Al/perovskite and Ag/perovskite stacking layers there are impurity peaks that cannot be assigned to perovskite, Al or Ag (Figure 5a), so a strong chemical reaction between them must have occurred. However, the Cu/perovskite stacking layer was much more stable. After storing in air for 20 h, the Cu layer on top of perovskite film remained shiny and intrinsic "copper red" color, and the XRD pattern of the sample does not show any impurity peaks (Figure 5a). The cross-sectional SEM images in Figure 5b shows that the stacking layer morphology of Cu/perovskite on glass substrate is clearly defined, with the perovskite layer remaining intact. In contrast, depositing Al on perovskite film ruins the perovskite layer morphology totally. It should be noted that though perovskite is more stable with Cu, the reaction between them in the ambient environment does occur slowly. The XRD pattern of the Cu/perovskite sample after storing in air for 20 d contains impurity peaks (Figure S6, Supporting Information). Nevertheless, in real devices an ETL is inserted between perovskite and Cu, which is able to suppress

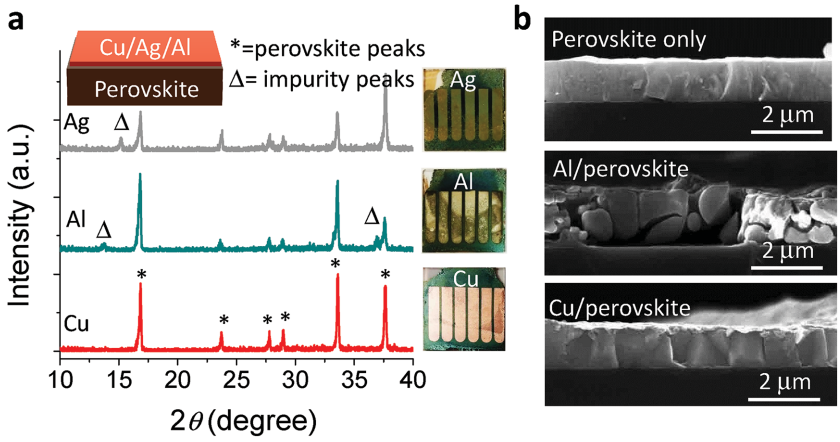

Figure 5. Stability comparison of Ag, Al, and Cu deposited directly on perovskite films. a) XRD of metal (Ag, Al, Cu)/perovskite stacking layers after storing in air for 20 h. Top left inset shows the sample structure and right column shows photographs of those samples. b) SEM images of pristine perovskite, Al/perovskite, and Cu/perovskite layers on glass substrate.

the reaction even at the interface level for more than 20 d, as evidenced by the device stability results.

In summary, perovskite solar cells with PCE > 18.0% and stability longer than 20–30 d in air for the unsealed devices were fabricated by the scalable doctor-blade coating method. The freedom of controlling parameters during the initial film formation stage (e.g., in situ temperature, precursor stoichiometry) to obtain high quality perovskite films with tunable composition demonstrates that the doctor-blade coating method can be a good supplement to spin-coating method, not only from scalable fabrication perspective but also for lab scale research. The discovery that Cu can be a more stable cathode metal than Al or Ag without sacrificing the device performance paves the way to further improve device long term stability.

Experimental Section

Mixed Cation Perovskite Precursor Solution Preparation: MAI and PbI_2 were dissolved in DMF to form the $MAPbI_3$ precursor solution (1 M). FAI and PbI_2 were dissolved in DMF to form the $FAPbI_3$ precursor solution (1 M). Then the two solutions were mixed in certain ratio to form $FA_xMA_{1-x}PbI_3$ precursor solution.

Device Fabrication: PTAA (Sigma-Aldrich) in toluene (2 mg mL^{-1}) was spin-coated onto the ITO substrates at 4000 rpm for 20 s and annealed in nitrogen atmosphere at 100 °C for 10 min. Then, the PTAA covered ITO substrates were treated by Argon plasma for 15 s and used immediately. The perovskite precursor solution (≈20 µL) was dropped onto PTAA-covered ITO substrate on a hot plate with temperature from 100 to 145 °C, and swiped linearly by a glass blade at a speed of 0.75 cm s^{-1}. The as-prepared perovskite films were then annealed at 100 °C for 30 min. After that, ICBA/1,2-Dichlorobenzene (DCB) solution (20 mg mL^{-1}) was spin-coated on top of the perovskite layer at 6000 rpm for 20 s, and the films were further thermally annealed at 100 °C for 30 min. All of the above experiments were conducted in N_2 glove box. Finally, C_{60} (20 nm), BCP (8 nm), and Cu (or Al, Au) electrode (80 nm) were deposited by thermal evaporation sequentially.

Device Characterization: XRD spectra were measured by a Rigaku D/Max-B Diffractometer with Co K_α radiation (1.788 Å). Absorption spectra were measured by a LAMBDA 1050 UV–vis–NIR Spectrophotometer. Top view and cross-section SEM images were obtained with a Quanta 200 FEG ESEM. *I–V* curves with different scanning directions at 0.1 V s^{-1} and steady photocurrent under maximum power output bias were measured with a source-meter (Keithley 2400) under simulated AM 1.5G irradiation by a Xenon lamp (Oriel 67005), which was calibrated by a silicon diode equipped with a Schott visible color glass filter (KG5 color filter). EQE was obtained with a Newport QE measurement kit.

Supporting Information

Supporting Information is available from the Wiley Online Library or from the author.

Acknowledgements

The authors thank the financial support from Office of Naval Research under award N00014-15-1-2713.

Received: February 20, 2016
Revised: March 4, 2016
Published online: April 4, 2016

[1] A. Kojima, K. Teshima, Y. Shirai, T. Miyasaka, *J. Am. Chem. Soc.* **2009**, *131*, 6050.
[2] W. S. Yang, J. H. Noh, N. J. Jeon, Y. C. Kim, S. Ryu, J. Seo, S. I. Seok, *Science* **2015**, *348*, 1234.
[3] T. M. Brenner, D. A. Egger, L. Kronik, G. Hodes, D. Cahen, *Nat. Rev. Mater.* **2016**, *1*, 15007.
[4] O. Malinkiewicz, A. Yella, Y. H. Lee, G. M. Espallargas, M. Graetzel, M. K. Nazeeruddin, H. J. Bolink, *Nat. Photonics* **2014**, *8*, 128.
[5] P. Docampo, J. M. Ball, M. Darwich, G. E. Eperon, H. J. Snaith, *Nat. Commun.* **2013**, *4*, 2761.
[6] C. Bi, Q. Wang, Y. Shao, Y. Yuan, Z. Xiao, J. Huang, *Nat. Commun.* **2015**, *6*, 7747.
[7] R. Søndergaard, M. Hösel, D. Angmo, T. T. Larsen-Olsen, F. C. Krebs, *Mater. Today* **2012**, *15*, 36.
[8] A. Sandström, H. F. Dam, F. C. Krebs, L. Edman, *Nat. Commun.* **2012**, *3*, 1002.
[9] A. T. Barrows, A. J. Pearson, C. K. Kwak, A. D. Dunbar, A. R. Buckley, D. G. Lidzey, *Energy Environ. Sci.* **2014**, *7*, 2944.
[10] H. Chen, Z. Wei, X. Zheng, S. Yang, *Nano Energy* **2015**, *15*, 216.
[11] J. H. Kim, S. T. Williams, N. Cho, C. C. Chueh, A. K. Y. Jen, *Adv. Energy Mater.* **2015**, *5*, 1401229.
[12] Y. Deng, E. Peng, Y. Shao, Z. Xiao, Q. Dong, J. Huang, *Energy Environ. Sci.* **2015**, *8*, 1544.
[13] K. Hwang, Y. S. Jung, Y. J. Heo, F. H. Scholes, S. E. Watkins, J. Subbiah, D. J. Jones, D. Y. Kim, D. Vak, *Adv. Mater.* **2015**, *27*, 1241.
[14] N. J. Jeon, J. H. Noh, Y. C. Kim, W. S. Yang, S. Ryu, S. I. Seok, *Nat. Mater.* **2014**, *13*, 897.
[15] N. J. Jeon, J. H. Noh, W. S. Yang, Y. C. Kim, S. Ryu, J. Seo, S. I. Seok, *Nature* **2015**, *517*, 476.
[16] Z. Xiao, C. Bi, Y. Shao, Q. Dong, Q. Wang, Y. Yuan, C. Wang, Y. Gao, J. Huang, *Energy Environ. Sci.* **2014**, *7*, 2619.
[17] T. A. Berhe, W.-N. Su, C.-H. Chen, C.-J. Pan, J.-H. Cheng, H.-M. Chen, M.-C. Tsai, L.-Y. Chen, A. A. Dubale, B.-J. Hwang, *Energy Environ. Sci.* **2016**, *9*, 323.
[18] T. Leijtens, G. E. Eperon, N. K. Noel, S. N. Habisreutinger, A. Petrozza, H. J. Snaith, *Adv. Energy Mater.* **2015**, *5*, 1500963.
[19] A. Guerrero, J. You, C. Aranda, Y. S. Kang, G. Garcia-Belmonte, H. Zhou, J. Bisquert, Y. Yang, *ACS Nano* **2016**, *10*, 218.
[20] J. You, L. Meng, T.-B. Song, T.-F. Guo, Y. M. Yang, W.-H. Chang, Z. Hong, H. Chen, H. Zhou, Q. Chen, *Nat. Nanotechnol.* **2016**, *11*, 75.
[21] W. Chen, Y. Wu, Y. Yue, J. Liu, W. Zhang, X. Yang, H. Chen, E. Bi, I. Ashraful, M. Grätzel, *Science* **2015**, *350*, 944.
[22] C. C. Stoumpos, C. D. Malliakas, M. G. Kanatzidis, *Inorg. Chem.* **2013**, *52*, 9019.
[23] J. W. Lee, D. J. Seol, A. N. Cho, N. G. Park, *Adv. Mater.* **2014**, *26*, 4991.
[24] Q. Han, S. H. Bae, P. Sun, Y. T. Hsieh, Y. M. Yang, Y. S. Rim, H. Zhao, Q. Chen, W. Shi, G. Li, Y. Yang, *Adv. Mater.* **2016**, *28*, 2253.
[25] Y. Deng, Q. Wang, Y. Yuan, J. Huang, *Mater. Horiz.* **2015**, *2*, 578.
[26] Z. A. Page, Y. Liu, V. V. Duzhko, T. P. Russell, T. Emrick, *Science* **2014**, *346*, 441.
[27] S. H. Oh, S. I. Na, J. Jo, B. Lim, D. Vak, D. Y. Kim, *Adv. Funct. Mater.* **2010**, *20*, 1977.
[28] V. Mihailetchi, P. Blom, J. Hummelen, M. Rispens, *J. Appl. Phys.* **2003**, *94*, 6849.
[29] V. D'Innocenzo, G. Grancini, M. J. Alcocer, A. R. S. Kandada, S. D. Stranks, M. M. Lee, G. Lanzani, H. J. Snaith, A. Petrozza, *Nat. Commun.* **2014**, *5*, 3586.
[30] Y. Deng, Z. Xiao, J. Huang, *Adv. Energy Mater.* **2015**, *5*, 1500721.

[31] Y. Yuan, J. Chae, Y. Shao, Q. Wang, Z. Xiao, A. Centrone, J. Huang, *Adv. Energy Mater.* **2015**, *5*, 1500615.
[32] Y. Yuan, J. Huang, *Acc. Chem. Res.* **2016**, *49*, 286.
[33] W. Nie, H. Tsai, R. Asadpour, J.-C. Blancon, A. J. Neukirch, G. Gupta, J. J. Crochet, M. Chhowalla, S. Tretiak, M. A. Alam, *Science* **2015**, *347*, 522.
[34] W. Zhou, Y. Zhao, C. Shi, H. Huang, J. Wei, R. Fu, K. Liu, D. Yu, Q. Zhao, *J. Phys. Chem. C* **2016**, *120*, 4759.
[35] G. E. Eperon, S. N. Habisreutinger, T. Leijtens, B. J. Bruijnaers, J. J. van Franeker, D. W. deQuilettes, S. Pathak, R. J. Sutton, G. Grancini, D. S. Ginger, *ACS Nano* **2015**, *9*, 9380.